SUPPLEMENTARY MATERIAL: Triggering proccesses in rock fracture

Jörn Davidsen,[1,2,*] Grzegorz Kwiatek,[2] Thomas Goebel,[3] Elli-Maria Charalampidou,[4] Sergei Stanchits,[5] Marc Rück,[2,6] and Georg Dresen[2,6]

[1] *Complexity Science Group, Department of Physics and Astronomy, University of Calgary, Canada*
[2] *GFZ German Research Centre for Geosciences, Section 3.2: Geomechanics and Rheology, Potsdam, Germany*
[3] *California Institute of Technology, Seismological Laboratory, Pasadena, United States*
[4] *Heriot–Watt University, Institute of Petroleum Engineering, Edinburgh, United Kingdom*
[5] *TerraTek, Salt Lake City, United States*
[6] *University of Potsdam, Potsdam, Germany*

(Dated: June 15, 2016)

We present more details on the experiments and an additional figure similar to Fig. 3 but for the case of shuffled catalogs. These are used to estimate the value n^*, which separates the two different populations of triggered events and background events. We also present additional figures for Westerly granite indicating that triggering of AE events by other acoustic emission events is basically absent even close to failure if no significant large-scale imperfection are present.

To record the AE activity, a 16-channel acquisition system operating at 10 MHz sampling rate was used [1, 2] allowing for a continuous detection of AE events even at high AE activity. As the AE events were processed in fixed time windows of 1024 samples, the shortest time interval in the experiments considered here between two consecutive events equaled 102.4 μs, yet the P-wave onset times of AE arrivals at each particular channel were determined with accuracy of about 0.5 μs.

AE events were located by inverting 10-14 P-wave onset times using grid search/simplex optimization technique and assuming a time-dependent 5-layered quasi-anisotropic velocity model [1, 3] leading to ± 2 mm location accuracy. The AE magnitude was calculated as [4]:

$$m = \log_{10} \sqrt{\frac{1}{n} \sum_{j=1}^{n} (A_j D_j)^2}, \tag{S1}$$

where A_i is the maximal amplitude of the P-wave pulse detected at sensor i corrected for the distance D_i between the AE event and the sensor. The magnitude of completeness $m_{\rm th}$ was identified as the lowest magnitude threshold for which the estimate of the b-value in the GR distribution became constant [5].

TABLE S1. List of analyzed experiments. Here, $\dot{u}$ is displacement rate (constant in almost all experiments), P_c is the confining pressure, $m_{\rm th}$ is the AE magnitude (Eq. (S1)) of completeness, T_i is the begin of observation period and T_f its end. The observation period was chosen such that transient artifacts and the failure itself were excluded and temporal resolution issues due to high activity rates were minimal. N is the number of AE events above m_{th} during that period.

name	large-scale imperfection	$\dot{u}$ [μm/min]	$P_c\,(\sigma_2 = \sigma_3)$ [MPa]	$m_{\rm th}$	T_i [s]	T_f [s]	N
Vo3	-	20	80	3.35	0	7400	4200
Be7a	notch, inclusion	20	160	3.25	0	4200	24163
Wgp01	-	20	75	2.35	0	8200	1658
Wgp01 (late)	-	varying (Fig. S2)	75	2.35	8200	8350	1281
Wgrn07	notch	20	75	2.35	0	5825	8114

* davidsen@phas.ucalgary.ca

[1] S. Stanchits, S. Vinciguerra, and G. Dresen, Pure and Applied Geophysics **163**, 975 (2006).
[2] E.-M. Charalampidou, S. Stanchits, G. Kwiatek, and G. Dresen, European Journal of Environmental and Civil Engineering , 1 (2014).

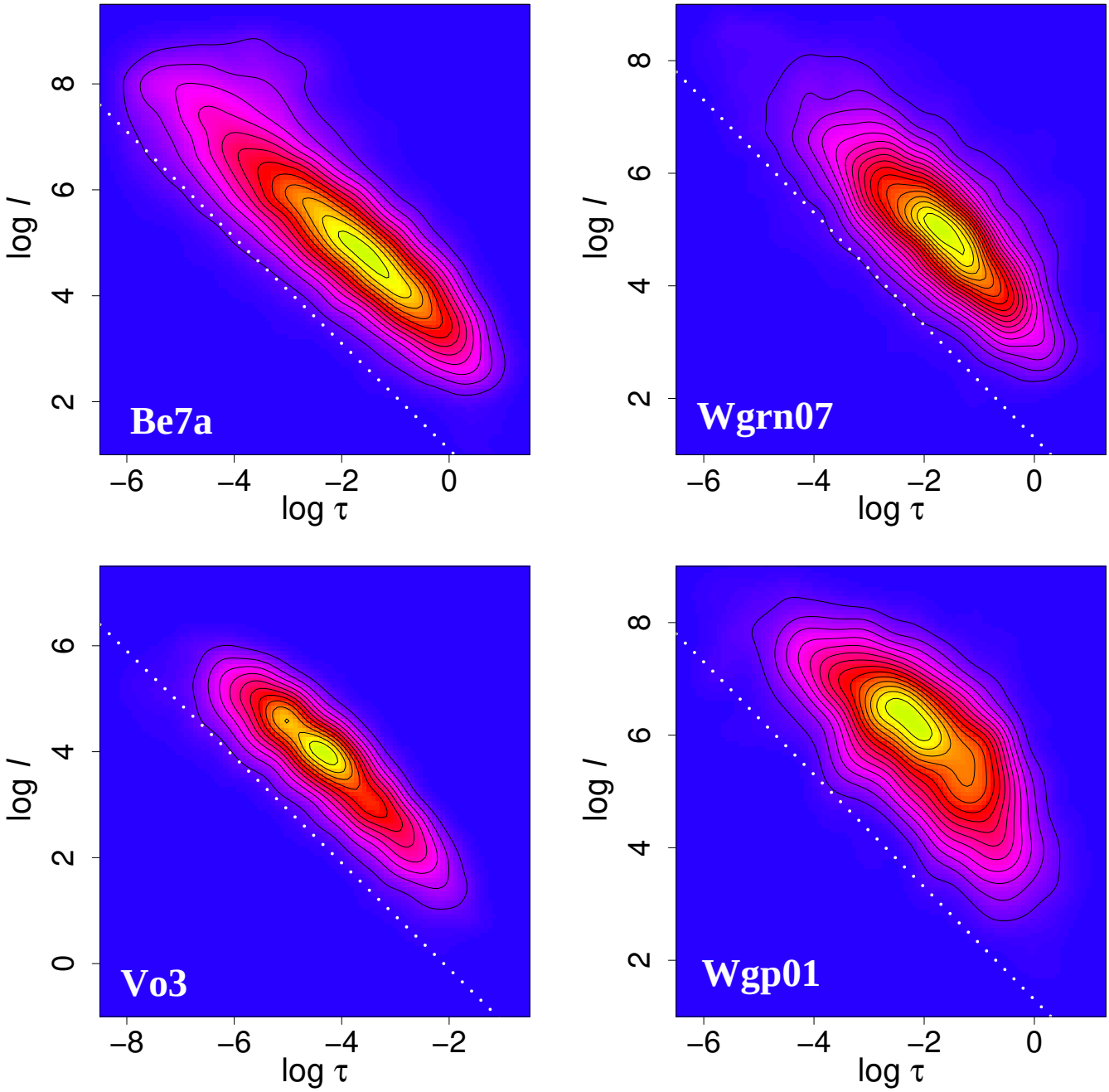

FIG. S1. (Color online) Density plots of the set $\{n_j^*\}$ for the shuffled catalogs of experiments with (upper left) and without (lower left) large scale imperfections (using $D_f = 2.3$ and the respective b-values (see, e.g., Fig. 3)) represented in $\log\tau$–$\log l$ space as defined in Eq. (2). Data are denser in yellow/red regions and tend to zero density in blue regions. Time is measured in seconds and distances are measured in millimeters. These plots are used to estimate the value n^* (shown as the straight line in the plots), which separates the two different populations of triggered events (below the line) and background events (above the line).

[3] G. Kwiatek, E.-M. Charalampidou, and G. Dresen, Int. J. Rock Mech. Min. Sci. **65**, 153 (2014).
[4] G. Kwiatek, T. H. W. Goebel, and G. Dresen, Geophys. Res. Lett. , 2014GL060159 (2014).
[5] J. Davidsen, C. Gu, and M. Baiesi, Geophysical Journal International **201**, 965 (2015).

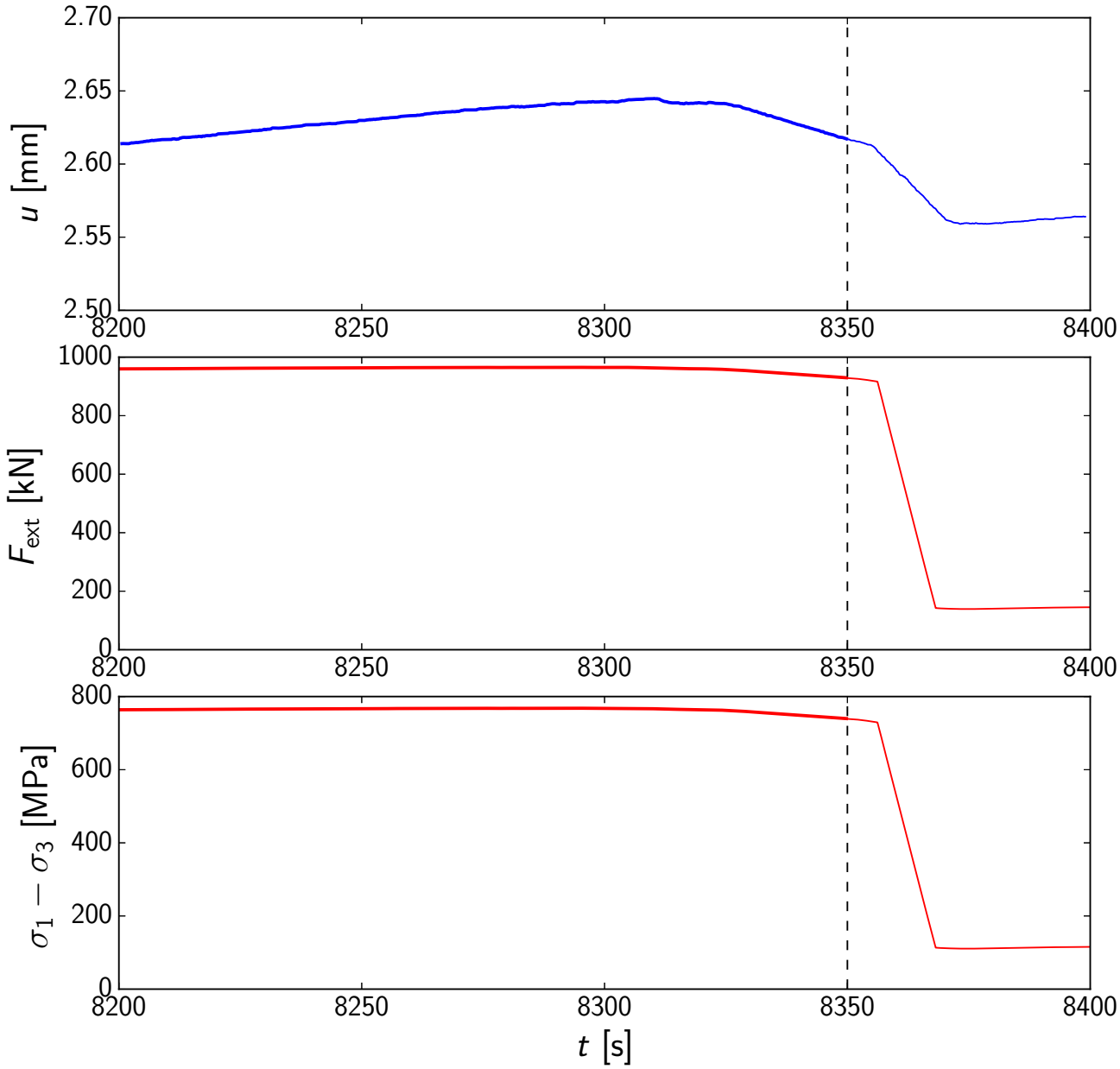

FIG. S2. (Color online) Wgp01: Temporal evolution of displacement, force and differential stress at late times. The time interval from 8200s to 8350s corresponds to Wgp01 (late). AE activity feedback control was used here to adjust the loading close to failure.

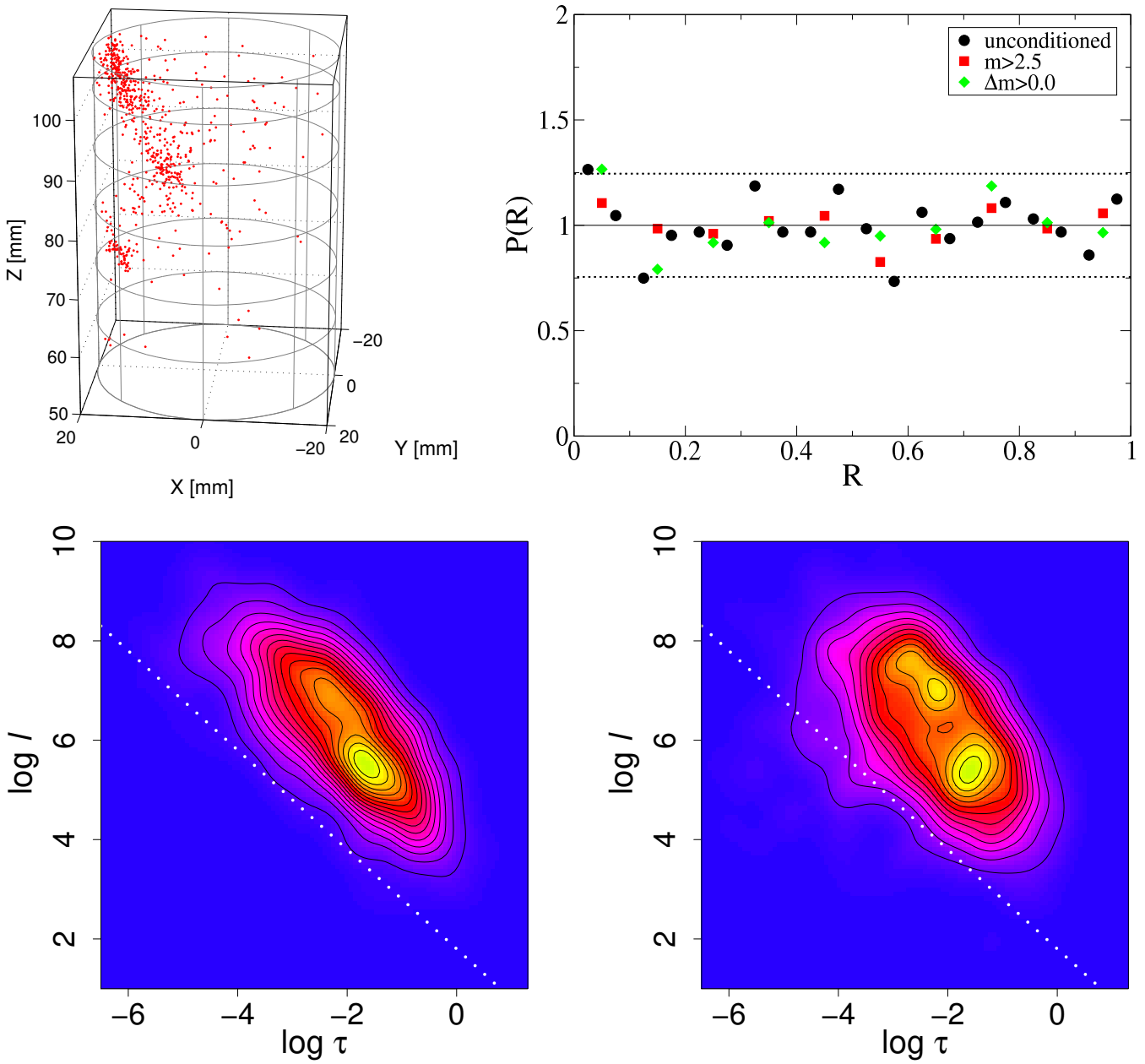

FIG. S3. (Color online) Wgp01 (late) close to failure (see Fig. S2 and Table S1): (a) Strong spatial localization of the AE activity. (b) PDF of the interevent time ratio for different conditions indicating weak or no temporal clustering (the dotted lines correspond to the 95% confidence intervals of a uniform distribution (based on Poissonian errors) for the unconditioned and the conditional $\Delta m > 0.0$ case, and correspond to the smallest uncertainties of all cases). (c) Density plots similar to Fig. S1, indicating that triggering is basically absent as observed far away from failure. (Left: Shuffled catalog. Right: Original catalog.)

TABLE S2. AE source types for the analyzed experiments.

name	(sub-) set	compression	shear	tensile
Vo3	all	84%	16%	0%
Be7a	all	99%	1%	0%
Be7a	trigger	99%	1%	0%
Be7a	triggered	99%	1%	0%
Be7a	background	99%	1%	0%
Wgp01	all	42%	22%	36%
Wgp01 (late)	all	61%	28%	11%
Wgrn07	all	68%	24%	8%
Wgrn07	trigger	78%	21%	1%
Wgrn07	triggered	77%	21%	2%
Wgrn07	background	66%	24%	10%